Synchronization and spatiotemporal patterns in coupled phase oscillators on a weighted planar network

Yuki Kagawa* and Atsuko Takamatsu
Department of Electrical Engineering and Bioscience, Waseda University, Tokyo 169-8555, Japan
(Received 8 September 2008; published 22 April 2009)

To reveal the relation between network structures found in two-dimensional biological systems, such as protoplasmic tube networks in the plasmodium of true slime mold, and spatiotemporal oscillation patterns emerged on the networks, we constructed coupled phase oscillators on weighted planar networks and investigated their dynamics. Results showed that the distribution of edge weights in the networks strongly affects (i) the propensity for global synchronization and (ii) emerging ratios of oscillation patterns, such as traveling and concentric waves, even if the total weight is fixed. In-phase locking, traveling wave, and concentric wave patterns were, respectively, observed most frequently in uniformly weighted, center weighted treelike, and periphery weighted ring-shaped networks. Controlling the global spatiotemporal patterns with the weight distribution given by the local weighting (coupling) rules might be useful in biological network systems including the plasmodial networks and neural networks in the brain.

DOI: 10.1103/PhysRevE.79.046216 PACS number(s): 05.45.Xt, 82.40.Ck, 87.90.+y

I. INTRODUCTION

During the past several years, many researchers have studied coupled dynamical systems on complex networks [1,2]. Most studies specifically examine the emergence of large-scale coherent behavior or synchronization. To date, it has been shown that the synchronizability of dynamical systems on complex networks is affected strongly by the small-world property of the networks, which is characterized by high clustering coefficients and small path lengths, and the heterogeneity in the degree (connectivity) distribution of the networks [3,4]. Synchronizability can be enhanced by changing strength and directionality of the couplings between dynamical systems based on knowledge of the network topology [5,6].

Many of these results are derived using systems of small-world and scale-free network models [7,8] representing complex relational networks, such as the world wide web, biochemical, and citation networks. A prominent feature of such models is the existence of vertices with very large degree. This implies that some vertices are connected to numerous other network vertices. Some theoretical studies of the synchronization of weighted networks are based on the assumption that vertices in the networks have large degrees [9,10].

However, degrees of the vertices in many real networks are not so large, particularly when the network is "planar," i.e., the vertices and the edges are embedded in a two-dimensional plane. Streets [11], railways [12,13], electric power grids [7], and ant-trail networks [14,15] are all examples of planar networks. In most cases of the planar networks, the highest degree is much smaller, and the largest path length is much larger than in nonplanar networks [16][1].

It is considered that coupled dynamical systems on such planar networks are difficult to synchronize because of their large path lengths. Therefore, in these systems, the connection strength between the systems on the vertices, or "weight" in the edges, becomes important to increase their synchronizability. Although it is known that the weights in the edges can increase the synchronizability in some systems on nonplanar networks whose minimum degrees are large [9,19], it is not clear what kind of weighting increases the synchronizability in the systems on planar networks.

Coupled dynamical systems on planar networks are found in several biological systems. A good example is the plasmodium of true slime mold, *Physarum polycephalum*, which spreads with developing tube networks on a two-dimensional plane (Fig. 1). Partial bodies of the plasmodium, whose cell thickness oscillates with a period of 1–2 min, interact mutually through protoplasmic streaming in the tubes that transport nutrients and other substances within the organism [20]. A prominent feature of these networks is the environmental dependency in their topology [21]. For example, the plasmodium develops treelike tube networks when the culture medium contains harmful chemicals such as KCl [Fig. 1(b)], whereas it develops latticelike ones when the medium contains oatmeal, which is food for this organism [Figs. 1(a) and 1(c)]. In addition to the change in the tube network topology, widths of the tubes, which are not uniform but distributed largely, are also changed. Because the tube width can be considered as the coupling strength in coupled biological oscillators of *Physarum* plasmodium [22,23], each edge in a plasmodium network has its own "weight" that is directly related to the coupling strength in the corresponding coupled dynamical systems. Therefore, dynamic oscillation patterns

*Present address: Institute for Nanoscience and Nanotechnology, Waseda University, Tokyo 162-8480, Japan; ykagawa@aoni.waseda.jp

[1]Note that some special planer networks, such as the Apollonian networks [17], can be scale-free and small-world simultaneously. Coupled dynamical systems on such networks have also been studied [18].

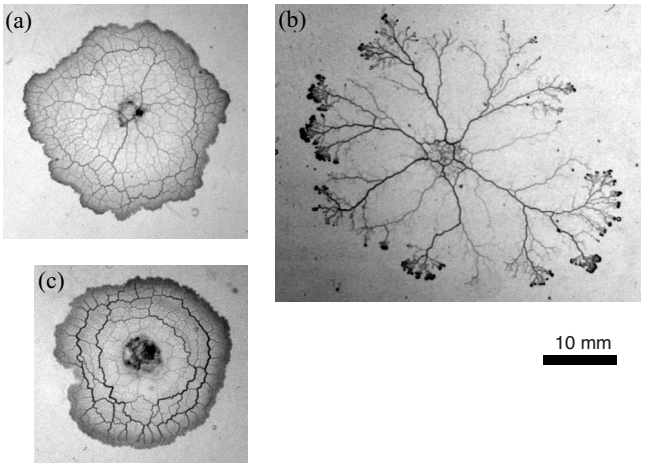

FIG. 1. Morphology of plasmodium of true slime mold. Tubular network structures observed on 0.9% agar media including [(a) and (c)] 10% (w/v) oatmeal extract and (b) 10 mM KCl. Bar, 10 mm.

observed in *Physarum* are thought to be controlled not only by the network topology, but also by the weight distribution on a network. The latter effects are of particular interest as a general problem.

Therefore, in this paper, we investigate the relation between the weight distribution in the edges of planar networks and the synchronization of coupled dynamical systems on the networks. We try to answer the following questions. (i) What kind of weight distribution on planar networks maximizes the probability for synchronization? (ii) What oscillation patterns emerge most frequently when the weight distributions are those observed in the tube networks of *Physarum*?

The paper is organized as follows. In Sec. II concrete models for coupled phase oscillators on weighted planar networks are introduced. In Sec. III numerical results of the model dynamics are presented by particularly addressing of the weight distribution on observed phase locking and oscillation patterns. In Sec. IV, necessary conditions are derived, by which the model systems show phase locking. In Sec. V, the biological relevance of the results described above is discussed in connection with the environment-dependent morphology of the plasmodium.

II. MODEL

Models for coupled phase oscillators on weighted planar networks are constructed as follows. First, weighted planar networks whose topology is an intermixture of tree and lattice are designed (Fig. 2). The intermixture network can express both tree and latticelike networks by controlling weight distribution in edges, as shown in Fig. 3. These networks mimic observed plasmodial tube networks. Next, simple weighting rules, with which the resulting weight distributions are symmetric, are given. By virtue of this simplicity, the weight distribution can be determined using only a few parameters. Finally, coupled phase oscillators are formulated based on the weight value in each edge of the network. Details of the topology design, the weighting rules including the definitions of the parameters, and the model equations to be solved are presented below.

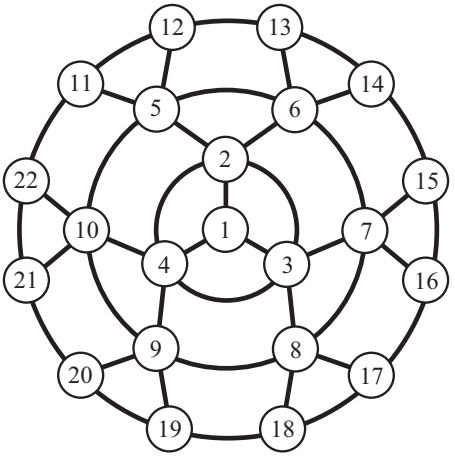

FIG. 2. Designed topology with $b=2$ and $d_{\max}=3$. Vertices are shown as open circles with indexing numbers.

A. Topology design

We design a network configuration that includes a tree as well as a lattice. Such a topology is generated by adding edges to a tree.

First, a "Cayley-tree," with the branching number of b and the maximum depth of $d_{\max}$, is generated. This is a regular tree in which every vertex not in the depth of $d_{\max}$ has degree (connectivity) $b+1$. The depth, d, of a given vertex is defined as the shortest path length from the root to the vertex. Therefore, the depth of the root vertex is zero ($d=0$). The number of vertices in depth d is given as

$$n(d) = (b+1)b^{d-1} \tag{1}$$

when $d \geq 1$. Consequently, this network has $N=1+\sum_{d=1}^{d_{\max}} n(d)=1+(b+1)(b^{d_{\max}}-1)/(b-1)$ vertices and $N-1$ edges. Next, we add edges by connecting the vertices in the

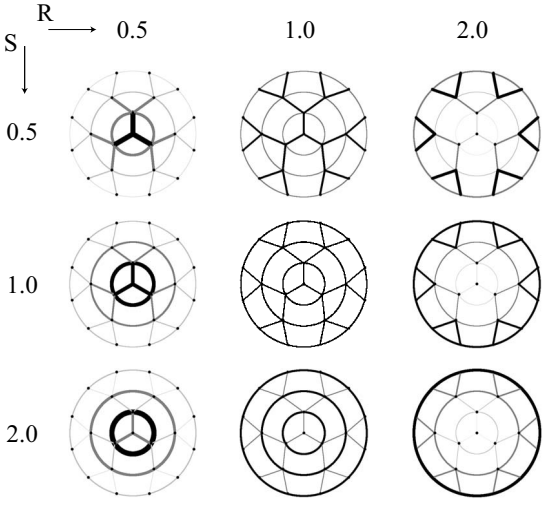

FIG. 3. Effect of the ratios R and S on the appearance of the weighted network with $b=2$ and $d_{\max}=3$.

same depth side by side to make a ring. In this process, $N-1$ edges are newly added, and all vertices but the root increase their degrees by two. The resulting topology with $b=2$ and $d_{\max}=3$ (and therefore $N=22$) is shown in Fig. 2.

Each vertex on the network can be indexed using a unique integer $i=1,2,\ldots,N$ such that shown in Fig. 2. Details of the indexing method and the connection rules are given in the Appendix.

B. Weighting rules

Each edge on the designed topology is weighted using simple symmetrical rules defined with only three parameters, R, S, and w_{tot}. The parameter R determines weight distributions among edges along the radial direction of the designed topology, and the parameter S determines the weights on the concentric edges. The parameter w_{tot} is the total weight, which is assumed to be constant during the observation of the phase dynamics. The definition of these three parameters is given in the following along with the relation between these weighting parameters and each edge weight in the network.

First, we separate the edges into two groups. The first group consists of $N-1$ edges in the radial direction. The second group consists of the remainder $N-1$ edges in the concentric direction. Below, weights on the edges belonging to the first and the second groups are, respectively, denoted by w and v. Second, we assume that the weights in the same depth are identical. Accordingly, the weights can be determined using a single parameter d, such that $w(d)$ and $v(d)$ are as described below. We define $w(d)$ as the weight on the edge that connects a vertex in depth $d-1$ and one in depth d. Similarly $v(d)$ is defined as the weight on the edge that connects vertices in the same depth d. Third, we define the parameters R and S as the ratio of weights in the depth $d+1$ to those in the depth d, and the ratio of weights in the concentric direction to those in the radial direction, respectively. Using w and v, these ratios are given as

$$R = \frac{w(d+1)}{w(d)} = \frac{v(d+1)}{v(d)} \tag{2}$$

and

$$S = \frac{v(d)}{w(d)}, \tag{3}$$

for any d. Similarly, the total weight w_{tot} is given as

$$w_{\text{tot}} = \sum_{d=1}^{d_{\max}} n(d)[w(d) + v(d)]. \tag{4}$$

For given R, S, and w_{tot}, all of the weights on the edges in the network with the branching number b and the maximum depth $d_{\max}$ are determined uniquely as

$$w(d) = \begin{cases} \dfrac{w_{\text{tot}} R^{d-1}(bR-1)}{(1+b)(1+S)[(bR)^{d_{\max}}-1]}, & bR \neq 1 \\ \dfrac{w_{\text{tot}} R^{d-1}}{d_{\max}(1+b)(1+S)}, & bR = 1, \end{cases} \tag{5}$$

and $v(d)=Sw(d)$ for $d=1,2,\ldots,d_{\max}$.

In Fig. 3, we present how the ratios R and S affect the appearance of one of the designed networks when w_{tot} is fixed. The parameter R determines the weight distribution along the radial direction. Weights in the center region are larger (smaller) than those in the periphery region when $R<1$ ($R>1$). Another parameter S determines whether the network is treelike or ringlike. The networks becomes treelike (ringlike) ones when $S<1$ ($S>1$). Treelike and ringlike networks are frequently found in the tube networks of the plasmodium [see Figs. 1(b) and 1(c), respectively]. When the special case of $R=S=1$, all the weights are identical, i.e., $w(d)=v(d)=w_{\text{tot}}/2(N-1)$, for $d=1,2,\ldots,d_{\max}$.

C. Coupled oscillators

On the weighted networks characterized by b, $d_{\max}$, R, S, and w_{tot}, coupled oscillators are constructed by putting an oscillator on each vertex of the network and coupling the nearest neighbors. As the oscillating units, we use phase oscillators [2,24]. Formulation of the dynamics of the coupled oscillator system is as shown below,

$$\frac{d\phi_i}{dt} = \omega_i + \sum_j A_{ij} \sin(\phi_j - \phi_i). \tag{6}$$

Therein, $\phi_i(t)$ represents the instantaneous phase of the oscillator on the vertex $i(=1,2,\ldots,N)$, ω_i is the natural frequency of the oscillator, and A_{ij} expresses the diffusive coupling strength between the vertices i and j. We assume that the coupling strength is directly proportional to the weights on the corresponding edge. Here, we set the proportional constant to be 1. Consequently, if vertices i and j are connected, $A_{ij}(=A_{ji})$ is given as (i) $A_{ij}=w(d)$ when these vertices are connected in the radial direction in depth $d-1$ and d, or (ii) $A_{ij}=v(d)$ when they are connected in the concentric direction in depth d.

III. RESULTS

We performed numerical calculation for the evolution of phases for coupled phase oscillators on weighted networks governed by Eq. (6) with the time step of 0.1. The network is designed to be $b=2$ and $d_{\max}=3$ so that the size $N=22$. The natural frequencies ω_i are chosen randomly with a Gaussian distribution with mean 1.0 and variance 0.01; the initial phases of the oscillators are given randomly from $[0,2\pi)$. The resulting data, i.e., time series of the phases $\phi_i(t), i=1,2,\ldots,N$, are used (i) to calculate the probability that the system shows phase locking P_{pl} and (ii) to estimate the emerging ratio of distinct spatiotemporal oscillation patterns in the systems on three typical weighted networks.

A. Phase locking

Phase locking between two phase oscillators ϕ_i and ϕ_j is fulfilled when the phase shift $\phi_i(t)-\phi_j(t)$ is time independent. The system shows global synchronization if all pairs of the oscillators in the network are phase locked.

To detect, numerically, the phase locking in the system, the phase shifts $\Delta\phi_i(t) \equiv \phi_i(t)-\phi_1(t), i=2,3,\ldots,N$ for 900

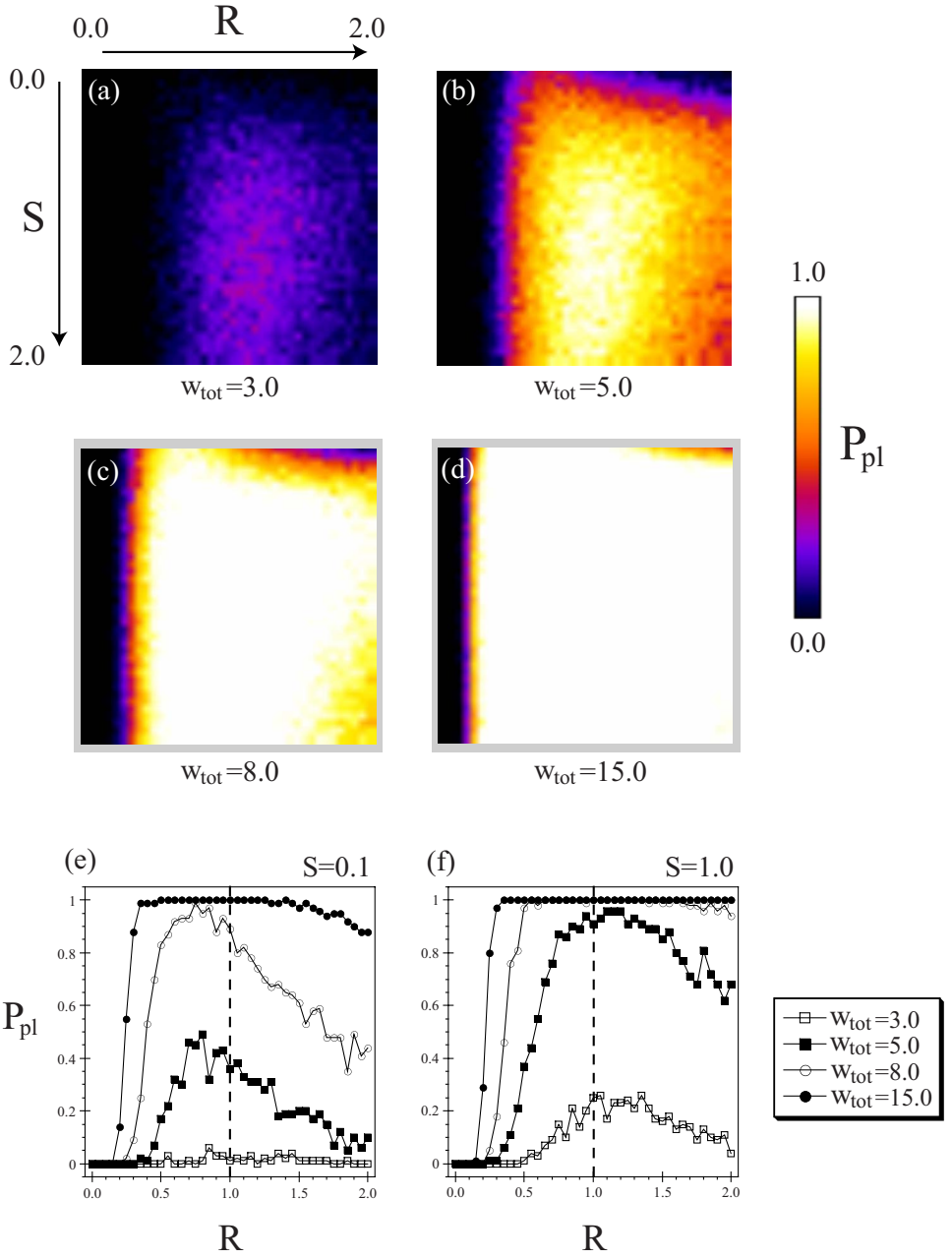

FIG. 4. (Color online) [(a)–(d)] Probability that the coupled phase oscillators on the weighted network show the phase locking (P_{pl}) calculated in the R-S space. Each probability for a given set of R and S is given by the number of samples showing the phase locking divided by the number of observations ($n=100$). $b=2, d_{\max}=3$, and (a) $w_{\mathrm{tot}}=3$, (b) 5, (c) 8, and (d) 15 are used. [(e) and (f)] P_{pl} shown against R when (e) $S=0.1$ and (f) 1.0 for $w_{\mathrm{tot}}=3$, 5, 8, and 15.

$<t\leq 1000$, and their *time variance*

$$\sigma^2_{\Delta\phi_i} \equiv \overline{[\Delta\phi_i(t) - \overline{\Delta\phi_i(t)}]^2} \tag{7}$$

are calculated. The time average in Eq. (7) is denoted by an overline, e.g.,

$$\overline{\Delta\phi_i(t)} = \frac{1}{T_2 - T_1}\int_{T_1}^{T_2} \Delta\phi_i(t)dt \tag{8}$$

with $T_1=900$ and $T_2=1000$, where $\Delta\phi_i$ (and $\overline{\Delta\phi_i}$) is defined in the region of $(-\pi,\pi]$. The condition $\Sigma_{i=2}^{N}\sigma^2_{\Delta\phi_i} < \epsilon(=0.01)$ is examined for each initial condition to determine the phase locking state practically[2].

Figure 4 shows the probability that the system shows phase locking (P_{pl}) in the parameter space of R and S for given total weights w_{tot}. In this figure, each probability is given by the number of trials showing the phase locking divided by the total number of trials ($n=100$) with random initial condition. When the total weight is small, for example

[2]The value of ϵ was chosen as follows. First we calculated the sum of Eq. (7), $\Sigma_{i=2}^{N}\sigma^2_{\Delta\phi_i}$, in the region we considered in this study (i.e., $w_{\mathrm{tot}}=3,5,8,15$ and $R,S=[0,2]$), and found that almost all ($>99\%$) of the sum are (i) less than 10^{-10} or (ii) more than 10^{-1}. Therefore it is reasonable to consider that a threshold defining phase synchronization resides in the region of $[10^{-10},10^{-1}]$. In the present study, we used $\epsilon=10^{-2}$. However, any value of ϵ between 10^{-10} and 10^{-1} makes little difference in subsequent results.

when $w_{tot}=3$, the system rarely shows phase locking, irrespective of the parameters [Fig. 4(a)]. On the other hand, when the total weight is large, such as $w_{tot}=15$, the system almost always shows phase locking, irrespective of the parameters [Fig. 4(d)]. When the total weight is moderate, such as $w_{tot}=5$ or 8, P_{pl} depends on the network morphology determined by the weight distribution [Figs. 4(b) and 4(c)].

As portrayed in Figs. 4(b) and 4(f), P_{pl} has its largest value at $R\sim 1$ and $S\sim 1$, implying that the coupled phase oscillators on uniformly weighted networks readily exhibit phase locking. On the other hand, in the region of $S\leq 0.1$, corresponding to treelike structures, the probability P_{pl} has its peak at $R\sim 0.8$ for a given small S [see Fig. 4(e)]. This peak location implies that for phase locking, center weighted tree or treelike networks are preferable to uniformly weighted (i.e., $R=1$) ones.

B. Oscillation patterns

To measure the degree of coherence of collective behavior, we calculated the order parameter K defined as the amplitude of the mean field [24]. We found that the system shows the highest coherency when R is approximately 1 and S is approximately 1 (data not shown). If the order parameter is very large (the largest value is 1), we can deduce from the value of K that all phases are almost identical, and the global in-phase locking pattern is realized in the system. However, generally, we cannot tell anything about the oscillation pattern realized in the system based only on the value of K.

Consequently, to reveal the relation between the network morphology and emerging oscillation patterns, we manually classified the oscillation patterns that are visible in a computer screen by displaying instantaneous phases on corresponding vertices on the network for every time step. Although these patterns are dependent on initial conditions, the weight distribution on a given network topology affects the emerging ratio for each pattern. We define three distinct oscillation patterns and manually classify observed spatiotemporal patterns into these three patterns and the others to check this. Then we calculate the emerging ratio for each defined pattern by counting quantities of observations.

We consider coupled phase oscillators on the following three weighted networks: (i) Uniformly weighted network (denoted as UW) ($R=S=1.0$); (ii) Center-weighted treelike network (CT) ($R=0.8$, $S=0.1$); (iii) Periphery-weighted ring-shaped network (PR) ($R=S=1.8$ with $w_{tot}=5.0$ on the topology of $b=2$ and $d_{max}=3$) [see Fig. 6(a)]. These two-dimensional weighted networks correspond to plasmodium networks observed in various conditions.

In coupled phase oscillator systems, we can observe three distinct oscillation patterns: the global in-phase locking (IP), the traveling wave (TW), and the concentric wave (CW) patterns. The first, IP, is the pattern in which phase shifts between any two oscillators are small. The TW pattern has a large phase gradient. Finally, CW is the pattern with large phase shifts between oscillators in the center region and in the periphery region.

We use an image of time-averaged phase shifts for a given initial condition to define these oscillation patterns rigorously. Each vertex in the image is gray scaled with the value of the time-averaged phase shift from the root, $\overline{\Delta\phi_i}$, which is given by Eq. (8) with $T_1=1000$ and $T_2=1100$ here. Example images are shown in Fig. 5.

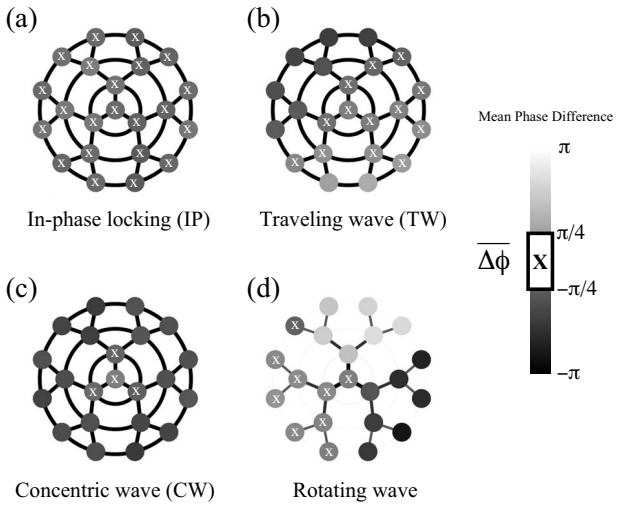

FIG. 5. Definition of the three distinct oscillation patterns based on images of $\overline{\Delta\phi_i}$. See text for the details of the definitions. [(a), (b), and (c)] Example images of $\overline{\Delta\phi_i}$ on the UW network, respectively, showing in-phase locking, traveling wave, and concentric wave patterns. (d) An image of $\overline{\Delta\phi_i}$ on the CT network showing rotating wave pattern. The "X" letters on the vertices represent that phase differences between these vertices and the root (or center) vertex are small. See text for the definition.

We consider that the phase shift is small and marked the vertex i with the "X" letter in these images when $|\overline{\Delta\phi_i}|<\pi/4$ is fulfilled. Based on the images of $\overline{\Delta\phi_i}$, we define the oscillation patterns IP, TW, and CW as follows. The oscillation pattern is defined as the pattern IP when more than 90% of the vertices are marked with the X letters, as in Fig. 5(a). The oscillation pattern is defined as the pattern TW when the vertices marked with Xs are clustered and sandwiched between the clustered vertices satisfying $\overline{\Delta\phi_i}\geq\pi/4$ and those satisfying $\overline{\Delta\phi_i}\leq-\pi/4$ such as Fig. 5(b), where the clustered vertices can be a single vertex. Pattern TW pertains when a pattern satisfies both definitions of patterns IP and TW. The oscillation pattern is defined as the pattern CW when the vertices marked with Xs are clustered and surrounded with the clustered vertices satisfying $\overline{\Delta\phi_i}\geq\pi/4$ or $\overline{\Delta\phi_i}\leq-\pi/4$, as shown in Fig. 5(c).

Using the above definitions, we classify 500 observations in coupled oscillators on each of the three weighted networks into the patterns IP, TW, and CW, or other (O). Results of the classification are displayed in Fig. 6(b). This figure clearly illustrates the differences in the emerging ratios for the defined oscillation patterns among the weighted networks of three types. In coupled oscillators on the UW network, global in-phase locking is observed more frequently than the traveling wave. The opposite relation holds when the CT network is used. Concentric wave patterns are visible frequently when the PR network is used. We also calculate the emerging ratios of the oscillation patterns under the condition of phase locking [see Fig. 6(c)]. In this figure, the largest emerging ratios of the patterns IP, TW, and CW are found,

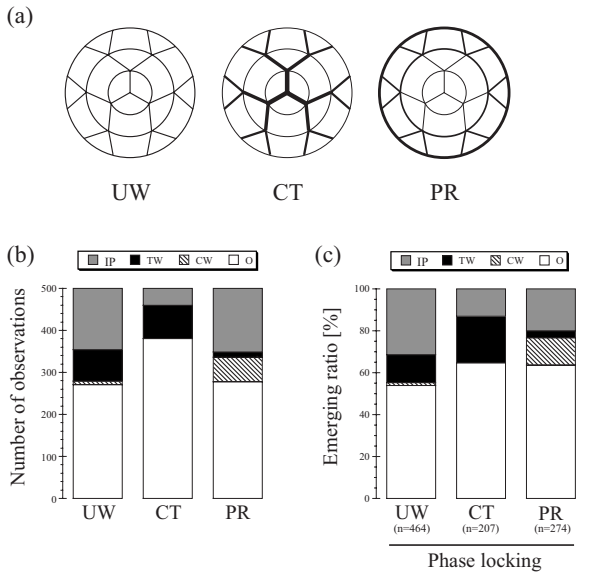

FIG. 6. (a) Schematic drawing of three typical networks used for classification of the oscillation patterns emerged on them. These weighted networks are constructed with the weighting parameters of $R=S=1.0$ (UW: uniformly weighted network), $R=0.8$ and $S=0.1$ (CT: center weighted treelike network), and $R=S=1.8$ (PR: periphery weighted ring-shaped network), on the topology of $b=2$ and $d_{\max}=3$. The acronyms UW, CT, and PR, respectively, correspond to the plasmodium networks portrayed in Figs. 1(a)–1(c). [(b) and (c)] Emerging ratio of the oscillation patterns found on the three weighted networks defined in (a). The oscillation patterns are in-phase locking (denoted as IP, gray), traveling wave (TW, black), and concentric wave (CW, striped) patterns. Also, O (white) includes all the other oscillation patterns. (b) All observations ($n=500$) include cases of non-phase-locking, or (c) only the samples showing the phase locking are used for the classification.

respectively, in coupled oscillators on the UW, CT, and PR networks.

The other distinct oscillation patterns, such as rotating wave [Fig. 5(d)], are found with small emerging ratios ($<3\%$). We classify these patterns in O here.

IV. NECESSARY CONDITION BY WHICH THE SYSTEM SHOWS PHASE LOCKING

In Fig. 4, we show that the weight distribution characterized by the parameters R and S drastically changes the probability for phase locking (P_{pl}), even if the network topology and the total weight w_{tot} remain unchanged. We also show that the UW network is preferable for phase locking.

In the following, we formally derive the necessary condition for phase locking, and show that the condition is less strict for the UW network. This implies that coupled oscillators on the UW network *can* exhibit phase locking with a large deviation among natural frequencies of its component oscillators, with which those on the other weighted networks *never* exhibit phase locking.

To derive the necessary condition, new variables $\theta_i \equiv \phi_i - \phi_r$ are introduced, where ϕ_r is the instantaneous phase of the reference oscillator. We can choose any oscillator as the reference. When coupled oscillators show phase locking, $\dot{\theta}_i = 0, i=1,2,\ldots,N$ are fulfilled. Using Eq. (6), these are rewritten as

$$\Delta\omega_i = -\sum_j A_{ij} \sin(\underline{\theta_j} - \underline{\theta_i}) + \sum_k A_{rk} \sin\underline{\theta_k}, \quad i = 1,2,\ldots,N, \tag{9}$$

where $\Delta\omega_i \equiv \omega_i - \omega_r$ is the difference between the natural frequency of oscillator i and that of the reference ($=\omega_r$). In addition, $\underline{\theta_i}$ is the phase difference in the phase locking state. If the solution $\underline{\theta_i}, i=1,\ldots,N$ exists, the following condition is satisfied:

$$|\Delta\omega_i| \le \left|\sum_j A_{ij} \sin(\underline{\theta_j} - \underline{\theta_i})\right| + \left|\sum_k A_{rk} \sin\underline{\theta_k}\right| \le \sum_j A_{ij} + \sum_k A_{rk} = s_i + s_r, \tag{10}$$

where $s_i \equiv \Sigma_j A_{ij}$ is the strength of the oscillator i, i.e., is the sum of the weights on the edges connecting to the vertex (oscillator). Therefore, $|\Delta\omega_i| \le s_i + s_r$ is the necessary condition for which the coupled oscillators show phase locking.

When natural frequencies $\omega_i, i=1,\ldots,N$ are given randomly with a Gaussian distribution with mean m and variance σ^2, the mean deviation is given as $\langle|\Delta\omega_i|\rangle = 2\sqrt{\sigma^2/\pi}$. Therefore, the necessary condition can be written as

$$\sqrt{\sigma^2} \le \frac{\sqrt{\pi}}{2} \min(s_i + s_r), \tag{11}$$

where $\min(s_i+s_r)$ is the minimum of the sum of arbitrary two strengths. Figures 7(a)–7(c), respectively, present the probability that the coupled oscillators on the UW, CT, and PR

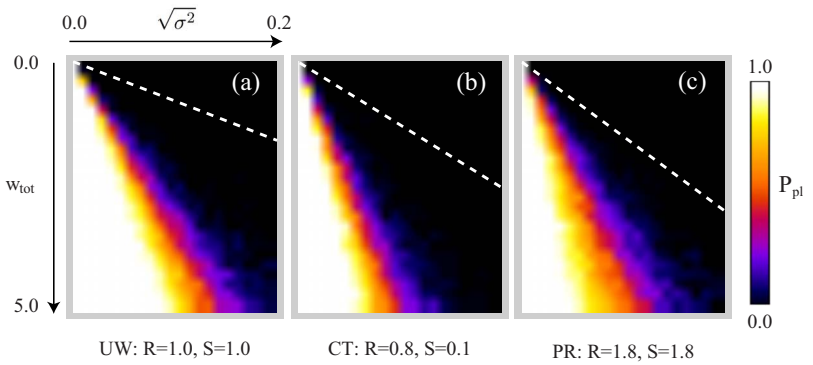

FIG. 7. (Color online) [(a), (b), and (c)] Probabilities that the coupled phase oscillators on the UW, CT, and PR networks, respectively, show phase locking, P_{pl}, calculated in the $\sqrt{\sigma^2}-w_{\mathrm{tot}}$ space. White dashed lines in the figures show boundaries of the region where the coupled oscillators satisfy the necessary condition for showing the phase locking. The regions include the lower-left corner.

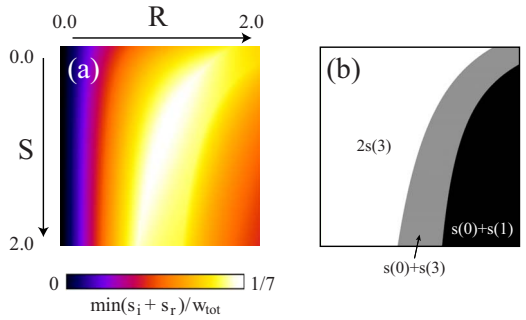

FIG. 8. (Color online) (a) Sum of the minimum and the second minimum of the strength, $\min(s_i+s_r)$, calculated in the R-S space. (b) Mathematical expressions for $\min(s_i+s_r)$ in the case of $b=2$ and $d_{\max}=3$. $s(d), d=0,1,3$ are given as Eq. (12).

networks exhibit phase locking (P_{pl}) for given $w_{\mathrm{tot}}=[0,5]$ and $\sqrt{\sigma^2}=[0,0.2]$. The corresponding necessary conditions, given by Eq. (11), are consistent with the numerical results (dashed lines in these figures). Moreover, the area satisfying the necessary condition for the system on the UW network is the largest, which is consistent with the numerical results.

When the sum of the minimum and the second minimum of the strength, i.e., $\min(s_i+s_r)$ in Eq. (11), is large, the necessary condition is less strict. Therefore, we can assume that coupled oscillators on the network show phase locking easily. In Fig. 8(a), we show the minimum of the sum of two strengths, $\min(s_i+s_r)$, on the R-S space. The sum has its maximum value at the point of $(R,S)=(1.0,1.0)$, where P_{pl} also has its maximum in Fig. 4(b). For nontreelike networks ($S>0.5$), the weight distribution of the probability for phase locking (P_{pl}) shown in Fig. 4(b) seems to be explained qualitatively with the necessary condition presented here.

Mathematical expressions for $\min(s_i+s_r)$ can be derived analytically for any given b and $d_{\max}$. When $b=2$ and $d_{\max}=3$ are used, the expressions in the region of $R=(0,2]$ and $S=[0,2]$ are given as $s(0)+s(1)$, $s(0)+s(3)$, and $2s(3)$ according to the regions shown in Fig. 8(b), where $s(d), d=0,1,\ldots$ are the strengths of the vertex in the depth d. Those are given as

$$s(d)=\begin{cases}(b+1)w(1), & d=0\\ (1+2S+bR)w(d), & d=1,2,\ldots,d_{\max}-1\\ (1+2S)w(d_{\max}), & d=d_{\max}.\end{cases} \tag{12}$$

In those equation, $w(d), d=1,2,\ldots,d_{\max}$ are given as Eq. (5).

V. DISCUSSION

As portrayed in Fig. 6, the weight distributions on a designed topology can control the emerging ratio for the spatiotemporal oscillation patterns. Coupled oscillators on UW networks preferably show a global in-phase locking pattern. Those on CT networks and PR networks preferably show traveling wave and the concentric wave patterns, respectively. Similarly, any other weighted network is inferred to have its own preferable oscillation patterns.

Such rules may be used by the tube network in the plasmodial true slime mold. In harmful conditions, the plasmodia are presumed to show traveling-wave patterns frequently because they develop treelike networks [Fig. 1(b)]. While in a pleasant condition, they are presumed to show global in-phase locking or concentric wave patterns because they develop latticelike networks [Fig. 1(a) or 1(c)], corresponding to the UW and PR networks. These predictions can be verified by experiments classifying oscillation patterns emerged on the tube networks and estimating emerging ratios for each pattern.

In the plasmodium, the TW patterns are known to emerge during tactic migration [25,26]. During this process, the phase wave propagated from the attractant and the phase gradient and the migration velocity are in the same direction [27]. Therefore, the high observation ratio of the TW patterns in a harmful condition is biologically relevant because this pattern can be regarded as migration toward the phase advance; the organism is expected to move away from the harmful place.

Conversely, we can presume that the plasmodium showing the CW patterns do not migrate but instead stay on the same place. In fact, the CW patterns are observed in a concentrically extending plasmodium [28]. Accordingly, showing the CW patterns in pleasant condition might also be biologically relevant because the organism can stay near the pleasant place.

Results of this study illustrate that the weight distribution, as determined by local weight ratios R and S, strongly affects the global synchronization and spatiotemporal oscillation patterns, even if the network topology is fixed. The control mechanism of the global spatiotemporal patterns by the local coupling strength might be useful in biological network systems including the plasmodial networks and neural networks in brain. In the latter networks, this implies the mechanism controlling firing patterns in brain by changing coupling strength between neurons. Such biological networks have physical substance. Therefore, changing their topology is expected to be much harder than changing weights on the edges. Changing the weight distribution is superior to changing the topology to control the system's global behavior at small cost or time. Therefore, to elucidate dynamic behaviors observed in such biological networks, monitoring temporal changes in the weight distribution must be necessary.

We have also studied dynamics of coupled logistic maps on weighted planar networks, whose topology and weighting rules are the same shown in the present study [29]. The probability finding phase synchronization [30] was calculated in the parameter space of R and S using a moderate total weight w_{tot}. As a result, it is found that the high probability region of phase synchronization resembles the one of phase locking shown in Fig. 4. In fact, coupled maps on uniformly weighted networks ($R\sim 1, S\sim 1$) show the highest probability of phase synchronization. Therefore we speculate that the relation between probability showing global synchronization and local coupling strength, or weight distribution in a given network, is less dependent on types of oscillators, i.e., whether the system is composed of phase oscillators or maps.

It might be necessary to extend the present simple model by introducing asymmetry in the network topology in addi-

tion to the weight distribution to model the dynamics of highly asymmetric and heterogeneous real biological networks. Time delays also demand consideration in the interactions between oscillators [23,31–33], and time evolutions in the weights (coupling strength) [34], for making specific models. These model extensions and investigation of the resulting dynamics are left as subjects for future work.

ACKNOWLEDGMENTS

This study was supported by a Grant-in-Aid for Scientific Research on Priority Areas "Emergence of Adaptive Motor Function through Interaction between Body, Brain and Environment" from the Japanese Ministry of Education, Culture, Sports, Science and Technology to A.T.

APPENDIX: RULES FOR INDEXING AND CONNECTING VERTICES IN THE NETWORK

Each vertex on the designed network can be indexed using a sequence of integers $\sigma=\{\alpha_0\alpha_1\alpha_2\cdots\alpha_d\}$, where d is the vertex depth. Actually, α_0 takes zero ($\alpha_0=0$), α_1 can take $0,1,\ldots,b$, and $\alpha_j (j\geq 2)$ can take $0,1,\ldots,b-1$. For example, the vertices numbered $1,2,\ldots,10$ in Fig. 2 are indexed, respectively, as {0}, {00}, {01}, {02}, {000}, {001}, {010}, {011}, {020}, and {021}. A vertex labeled by σ can have a unique integer index $i(\sigma)=i(\alpha_0,\alpha_1,\ldots,\alpha_d)=1,2,\ldots,N$ using the following rules: $i(0)=1$ and

$$i(0,\alpha_1,\alpha_2,\ldots,\alpha_d)=1+\alpha_d+\sum_{\delta=1}^{d-1}\alpha_\delta b^{d-\delta}+\nu_b(d-1), \tag{A1}$$

where

$$\nu_b(d)=1+\frac{b+1}{b-1}(b^d-1). \tag{A2}$$

Furthermore, $\nu_b(d)$ represents the number of vertices whose depths are less than or equal to d. Using this function, the total number of vertices can be expressed as $N=\nu_b(d_{\max})$. Similar indexing methods have appeared in previous reports [35,36].

The relation between σ and i is unique. Therefore, we can inversely derive σ as a function i, i.e., $\sigma(i)$. Using this notation, connections between vertices in the designed network can be described as follows: the root, indexed as $\sigma(1)=\{0\}$, is connected to $b+1$ vertices ("daughters"), whose indices are $\sigma(2+\alpha_1)=\{0\alpha_1\}$ with $\alpha_1=0,1,\ldots,b$; a vertex indexed as $\sigma(j)=\{\alpha_0\alpha_1\cdots\alpha_d\}$ (where $j\neq 1$ or $d\geq 1$) is connected to the "mother" vertex indexed as $\{\alpha_0\alpha_1\cdots\alpha_{d-1}\}$ and its "daughters" indexed as $\{\alpha_0\alpha_1\cdots\alpha_d\alpha_{d+1}\}$ with $\alpha_{d+1}=0,1,\ldots,b-1$, if they exist. The $\sigma(j)$ vertex is also connected to its "sisters" (or "cousins" sometimes) indexed as $\sigma(j_{nn})$ with $j_{nn}=j\pm 1$, when j is not the minimum [i.e., $\nu_b(d-1)+1$] or the maximum [i.e., $\nu_b(d)$] index in the present depth d. If $j=\nu_b(d-1)+1$, then j_{nn} is expected to be $j+1$ and $\nu_b(d)$; if $j=\nu_b(d)$, then j_{nn} is expected to be $j-1$ and $\nu_b(d-1)+1$. For example, when $b=2$ and $j=2$ (the minimum in the depth of $d=1$), then j_{nn} is expected to be 3 and $\nu_2(1)=4$. Consequently, the vertex $\sigma(2)$ is connected to the vertices $\sigma(3)$ and $\sigma(4)$, as well as the mother $\sigma(1)$ and the daughters $\sigma(5)$ and $\sigma(6)$ (see also Fig. 2).

[1] S. Boccaletti, V. Latora, Y. Moreno, M. Chavez, and D. Hwang, Phys. Rep. **424**, 175 (2006).
[2] G. Osipov, J. Kurths, and C. Zhou, *Synchronization in Oscillatory Networks* (Springer, Berlin, 2007).
[3] M. Barahona and L. M. Pecora, Phys. Rev. Lett. **89**, 054101 (2002).
[4] T. Nishikawa, A. E. Motter, Y. C. Lai, and F. C. Hoppensteadt, Phys. Rev. Lett. **91**, 014101 (2003).
[5] A. Motter, C. Zhou, and J. Kurths, Europhys. Lett. **69**, 334 (2005).
[6] M. Chavez, D. U. Hwang, A. Amann, H. G. E. Hentschel, and S. Boccaletti, Phys. Rev. Lett. **94**, 218701 (2005).
[7] D. Watts and S. Strogatz, Nature (London) **393**, 440 (1998).
[8] A. Barabási and R. Albert, Science **286**, 509 (1999).
[9] C. Zhou, A. E. Motter, and J. Kurths, Phys. Rev. Lett. **96**, 034101 (2006).
[10] J. G. Restrepo, E. Ott, and B. R. Hunt, Phys. Rev. Lett. **96**, 254103 (2006).
[11] A. Cardillo, S. Scellato, V. Latora, and S. Porta, Phys. Rev. E **73**, 066107 (2006).
[12] P. Sen, S. Dasgupta, A. Chatterjee, P. A. Sreeram, G. Mukherjee, and S. S. Manna, Phys. Rev. E **67**, 036106 (2003).
[13] J. Sienkiewicz and J. A. Holyst, Phys. Rev. E **72**, 046127 (2005).
[14] J. Buhl, J. Gautrais, R. Solé, P. Kuntz, S. Valverde, J. Deneubourg, and G. Theraulaz, Eur. Phys. J. B **42**, 123 (2004).
[15] J. Buhl, J. Gautrais, J. Louis Deneubourg, P. Kuntz, and G. Theraulaz, J. Theor. Biol. **243**, 287 (2006).
[16] M. Gastner and M. Newman, Eur. Phys. J. B **49**, 247 (2006).
[17] J. S. Andrade, H. J. Herrmann, R. F. S. Andrade, and L. R. da Silva, Phys. Rev. Lett. **94**, 018702 (2005).
[18] P. G. Lind, J. A. C. Gallas, and H. J. Herrmann, Phys. Rev. E **70**, 056207 (2004).
[19] D. Li, M. Li, J. Wu, Z. Di, and Y. Fan, Eur. Phys. J. B **57**, 423 (2007).
[20] N. Kamiya, Annu. Rev. Plant Physiol. **32**, 205 (1981).
[21] A. Takamatsu, E. Takaba, and G. Takizawa, J. Theor. Biol. **256**, 29 (2009).
[22] A. Takamatsu, T. Fujii, H. Yokota, K. Hosokawa, T. Higuchi, and I. Endo, Protoplasma **210**, 164 (2000).
[23] A. Takamatsu, T. Fujii, and I. Endo, Phys. Rev. Lett. **85**, 2026 (2000).
[24] Y. Kuramoto, *Chemical Oscillations, Waves, and Turbulence* (Springer, Berlin, 1984).
[25] Z. Hejnowicz and K. Wohlfarth-Bottermann, Planta **150**, 144 (1980).

[26] K. Matsumoto, T. Ueda, and Y. Kobatake, J. Theor. Biol. **122**, 339 (1986).
[27] Y. Miyake, S. Tabata, H. Murakami, M. Yano, and H. Shimizu, J. Theor. Biol. **178**, 341 (1996).
[28] T. Ueda, K. Matsumoto, T. Akitaya, and Y. Kobatake, Exp. Cell Res. **162**, 486 (1986).
[29] Y. Kagawa and A. Takamatsu, e-print arXiv:0904.1456v1.
[30] S. Jalan and R. E. Amritkar, Phys. Rev. Lett. **90**, 014101 (2003).
[31] F. M. Atay, J. Jost, and A. Wende, Phys. Rev. Lett. **92**, 144101 (2004).
[32] C. Masoller and A. C. Martí, Phys. Rev. Lett. **94**, 134102 (2005).
[33] P. Lind, A. Nunes, and J. Gallas, Physica A **371**, 100 (2006).
[34] A. Tero, R. Kobayashi, and T. Nakagaki, J. Theor. Biol. **244**, 553 (2007).
[35] P. M. Gade, H. A. Cerdeira, and R. Ramaswamy, Phys. Rev. E **52**, 2478 (1995).
[36] M. G. Cosenza and K. Tucci, Phys. Rev. E **64**, 026208 (2001).